

## Feedforward deformation control of a dielectric elastomer actuator based on a nonlinear dynamic model

Guo-Ying Gu, Ujjaval Gupta, Jian Zhu, Li-Min Zhu, and Xiang-Yang Zhu

Citation: [Applied Physics Letters](#) **107**, 042907 (2015); doi: 10.1063/1.4927767

View online: <http://dx.doi.org/10.1063/1.4927767>

View Table of Contents: <http://scitation.aip.org/content/aip/journal/apl/107/4?ver=pdfcov>

Published by the [AIP Publishing](#)

---

### Articles you may be interested in

[The dielectric breakdown limit of silicone dielectric elastomer actuators](#)

Appl. Phys. Lett. **104**, 052905 (2014); 10.1063/1.4863816

[Computational model of deformable lenses actuated by dielectric elastomers](#)

J. Appl. Phys. **114**, 104104 (2013); 10.1063/1.4821028

[Large actuation and high dielectric strength in metallized dielectric elastomer actuators](#)

Appl. Phys. Lett. **100**, 182901 (2012); 10.1063/1.4709480

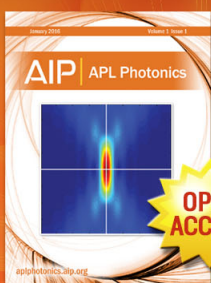
[Electromechanical stability in charge-controlled dielectric elastomer actuation](#)

Appl. Phys. Lett. **99**, 244101 (2011); 10.1063/1.3670048

[Large deformation and electromechanical instability of a dielectric elastomer tube actuator](#)

J. Appl. Phys. **108**, 074113 (2010); 10.1063/1.3490186

---



Launching in 2016!  
The future of applied photonics research is here

AIP | APL  
Photonics

# Feedforward deformation control of a dielectric elastomer actuator based on a nonlinear dynamic model

Guo-Ying Gu,<sup>1,2</sup> Ujjaval Gupta,<sup>2</sup> Jian Zhu,<sup>2,a)</sup> Li-Min Zhu,<sup>1</sup> and Xiang-Yang Zhu<sup>1</sup>

<sup>1</sup>State Key Laboratory of Mechanical System and Vibration, School of Mechanical Engineering, Shanghai Jiao Tong University, Shanghai 200240, China

<sup>2</sup>Department of Mechanical Engineering, National University of Singapore, 9 Engineering Drive 1, 117575 Singapore

(Received 24 May 2015; accepted 22 July 2015; published online 30 July 2015)

In the practical applications of actuators, the control of their deformation or driving force is a key issue. Most of recent studies on dielectric elastomer actuators (DEAs) focus on issues of mechanics, physics, and material science, whereas less importance is given to the control of these soft actuators. In this paper, we underline the importance of a nonlinear dynamic model as the basis for a feedforward deformation control approach of a rubber-based DEA. Experimental evidence shows the effectiveness of the feedforward controller. The present study confirms that a DEA's trajectory can be finely controlled with a solid nonlinear dynamic model despite the presence of material nonlinearities and electromechanical coupling. The effective control of DEAs may pave the way for extensive emerging applications to soft robots. © 2015 AIP Publishing LLC.

[<http://dx.doi.org/10.1063/1.4927767>]

The emerging field of soft robotics offers the prospect of applying soft actuators as artificial muscles in the robots, replacing traditional actuators based on hard materials, such as electric motors and piezoceramic actuators. Dielectric elastomers are one class of soft actuators, which can deform in response to voltage and can resemble biological muscles in the aspects of large deformation, high energy density, and fast response.<sup>1–3</sup>

Recent research into dielectric elastomers has mainly focused on issues regarding mechanics, physics, material designs, and mechanical designs.<sup>4–6</sup> For example, dielectric elastomer actuators (DEAs) are found to achieve giant voltage-induced deformation with an area strain greater than 1000%.<sup>7–9</sup> Materials are designed for both electrode and elastomer to improve the performance of DEAs.<sup>10–13</sup> The soft actuators with different mechanical designs can achieve various deformations and movements, thus realizing different functions. Recently, we have employed DEAs as artificial muscles to drive a jellyfish robot, a worm-like robot, and a human-face model.<sup>14</sup> The control of actuators is one of the key issues in developing robots. Strong nonlinearities due to large deformation and electromechanical coupling make control of the DEAs challenging. Extensive studies had been conducted to control traditional actuators, say, electric motors<sup>15</sup> or piezoceramic actuators.<sup>16</sup> However, to date, there has been much less research into control of the DEAs.<sup>17–22</sup>

This paper focuses on feedforward control of a DEA. We underline the importance of a nonlinear dynamic model as the basis for the feedforward deformation control approach. The desired deformation is first input into the controller, and then the controller generates the voltage to determine the actuator's deformation (Fig. 1). Experimental evidence shows that the DEA can track the desired

trajectories effectively despite the presence of material nonlinearities and electromechanical coupling. The effective control of DEAs may pave the way for extensive emerging applications to soft robots.

Figure 1(a) shows a schematic of a DEA, which is simple but has a practical application—inducing vibration for tactile feedback.<sup>23,24</sup> In the reference state (Fig. 1(a-i)), the membrane of a dielectric elastomer is not subject to any mechanical and electrical loads. Part A and Part B have the length  $L_{1A} = L_{1B}$  ( $= 10$  mm), and the width  $L_2$  ( $= 50$  mm). In the prestretched state (Fig. 1(a-ii)), the membrane is prestretched with  $\lambda_{1p} = 2$  and  $\lambda_{2p} = 2$ , and the two boundaries along the width are fixed by two frames. A rigid mass, which may function as a vibration shaker, is attached in the middle of the membrane to separate it into Part A and Part B. Part A is smeared with carbon grease as the compliant electrodes, while Part B is not. In a current actuated state (Fig. 1(a-iii)), Part A functions as an actuator and expands when subject to voltage ( $\Phi$ ), leading to the shrinking of Part B, thereby displacing the vibration shaker. As a result, Part A and Part B have the same width  $\lambda_{2p}L_2$ , but different lengths  $\lambda_{1A}L_{1A}$  and  $\lambda_{1B}L_{1B}$ , respectively, where  $\lambda_{1A}$  or  $\lambda_{1B}$  is the stretch in direction 1 of Part A or Part B. In the experiments, we employ a natural rubber, Oppo Band, Singapore (with a thickness  $H = 0.47$  mm) as the dielectric elastomer, since it exhibits low viscoelasticity and large reversible deformation.<sup>25</sup> A PCI-6014 control board equipped with the BNC-2120 interface (NI Corp.) is adopted to generate voltage, which is then amplified by a high voltage amplifier (10/40 A, Trek). A laser displacement sensor (ILD1700, Micro Epsilon) is employed to measure the real-time displacement of the actuator.

We develop a dynamic model as follows. As shown in Fig. 2(a), the system consists of three components: Part A (with the electrodes), Mass  $m$ , and Part B (without the electrode). For Mass  $m$ , the equation of motion is given by

<sup>a)</sup>Author to whom correspondence should be addressed. Electronic mail: mpezhu@nus.edu.sg

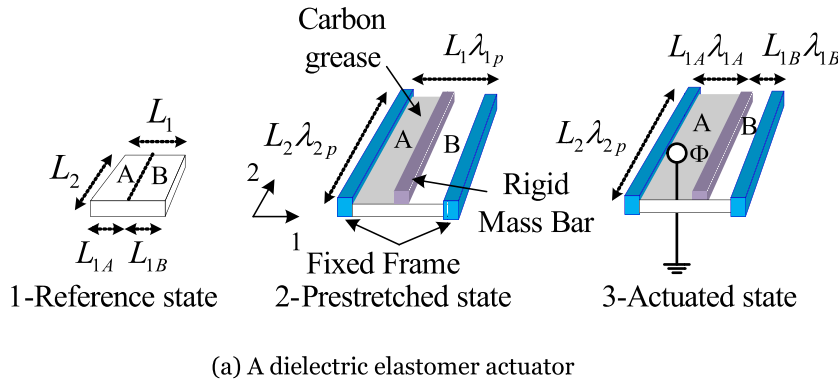
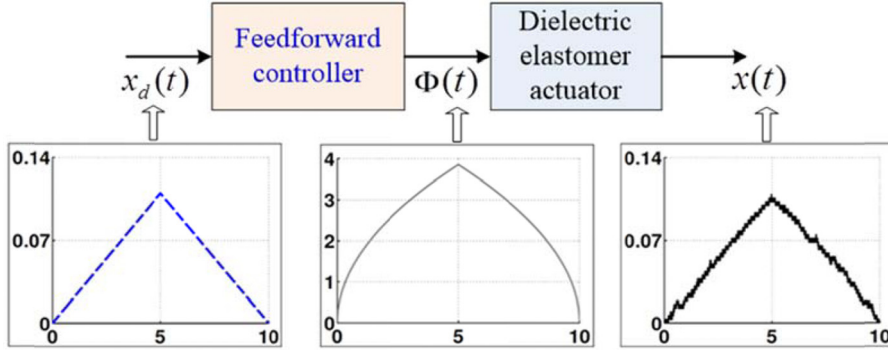


FIG. 1. (a) Schematic of the dielectric elastomer actuator. In the reference state (a-i), the elastomer is free of mechanical and electrical loads. In the prestretched state (a-ii), the elastomer is subject to bi-axial prestretches  $\lambda_{1p}$  and  $\lambda_{2p}$ , and the two boundaries are fixed by two frames. A rigid mass bar is attached to the elastomer to separate it into Part A and Part B. Part A is smeared with carbon grease as the compliant electrodes. In a current actuated state (a-iii), Part A is subject to voltage and expands. As a result, Part B shrinks and the mass moves. (b) Block diagram of the feedforward deformation controller.  $x_d(t)$  represents the desired trajectory,  $\Phi(t)$  represents the control voltage generated by the feedforward controller, and  $x(t)$  represents the deformation of the actuator.



$mL_{1A} \frac{d^2 \lambda_{1A}}{dt^2} = F_B - F_A - cL_{1A} \frac{d\lambda_{1A}}{dt}$ , where  $F_B$  is applied by Part B,  $F_A$  is applied by Part A, and  $t$  is time. For simplicity, we assume that the damping force applied to the vibration shaker is proportional to its velocity, that is  $F_f = -cL_{1A} \frac{d\lambda_{1A}}{dt}$ , where  $c$  is the damping coefficient. For Part A, the equation of motion is given by  $F_A = \mu(\lambda_{1A} - \lambda_{1A}^{-3} \lambda_{2p}^{-2})L_2H - \varepsilon \lambda_{1A} \frac{2p^2}{\lambda} \left(\frac{\Phi}{H}\right)^2 L_2H + \frac{1}{3} \rho L_{1A}^2 \frac{d^2 \lambda_{1A}}{dt^2} L_2H$ , where  $\mu$  is the small-strain

shear modulus,  $\varepsilon$  is the permittivity, and  $\rho$  is the density of the elastomer.<sup>26</sup> The first term in the above equation represents the elastic restoring force. The elastomer is taken to be incompressible, i.e.,  $\lambda_1 \lambda_2 \lambda_3 = 1$ , where  $\lambda_1$ ,  $\lambda_2$ , and  $\lambda_3$  are the stretches in the length, width, and thickness directions, respectively. Since the displacement of the actuator is not large (Fig. 2(b)), for simplicity, we assume that the elastomer is a neo-Hookean material with an elastic energy density  $W(\lambda_1, \lambda_2) = \frac{\mu}{2}(\lambda_1^2 + \lambda_2^2 + \lambda_1^{-2} \lambda_2^{-2} - 3)$ . Taking the first derivative of the elastic energy density with respect to  $\lambda_1$ , we can get the nominal elastic restoring stress.<sup>27</sup> The second term is the force induced by voltage (or the Maxwell stress), and the third term is the inertia force. For Part B where the voltage is absent, the equation of motion is given by  $F_B = \mu(\lambda_{1B} - \lambda_{1B}^{-3} \lambda_{2p}^{-2})L_2H + \frac{1}{3} \rho L_{1B}^2 \frac{d^2 \lambda_{1B}}{dt^2} L_2H$ . The first term in the equation is the elastic restoring force, and the second term is the inertia force. Since the distance between the two frames is fixed (Fig. 1(a)), we have  $\lambda_{1A} + \lambda_{1B} = 2\lambda_{1p}$ . Combining the equations of motion for Mass  $m$ , Part A, and Part B, we obtain the equation of motion of the system as follows

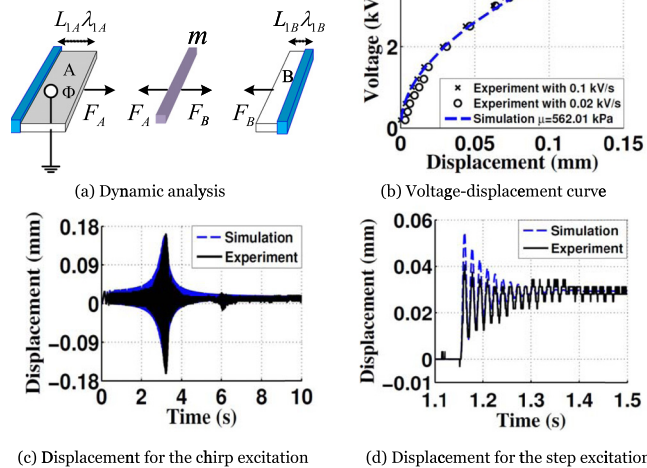


FIG. 2. (a) Dynamic analysis of the system. (b) The DC voltage as a function of the displacement of the actuator. The black crosses or circles represent the experimental data for a voltage ramp rate of 0.1 kV/s or 0.02 kV/s, respectively, and the dashed blue curve represents the calculations with  $\mu = 562.01$  kPa and  $\varepsilon = 2.39 \times 10^{-11} F/m$ . (c) The displacement of the actuator as a function of time for a chirp excitation. The solid black curve represents the experimental data, while the dashed blue curve represents the calculations with  $M = 17.5$  g and  $c = 0.696$  Ns/m. (d) The displacement of the actuator as a function of time for a step excitation.

$$M \frac{d^2 \lambda_{1A}}{dt^2} + c \frac{d\lambda_{1A}}{dt} - \frac{L_2H}{L_{1A}} \mu (2\lambda_{1p} - 2\lambda_{1A} - (2\lambda_{1p} - \lambda_{1A})^{-3} \lambda_{2p}^{-2} + \lambda_{1A}^{-3} \lambda_{2p}^{-2}) - \frac{L_2H}{L_{1A}} \varepsilon \lambda_{1A} \lambda_{2p}^2 \left(\frac{\Phi}{H}\right)^2 = 0, \quad (1)$$

where  $M (= m + \rho L_1 L_2 H / 3)$  is the effective mass of the system. This system is a typical nonlinear dynamic system. First, the material is nonlinear. In addition, voltage is

coupled with the deformation, known as parametric excitation.<sup>28,29</sup>

The material and physical parameters in Eq. (1), which include the effective mass  $M$ , the damping coefficient  $c$ , the shear modulus  $\mu$ , and the permittivity  $\varepsilon$ , can be identified as follows. Kaltseis *et al.* measured the permittivity of the elastomer as  $\varepsilon = 2.39 \times 10^{-11} F/m$ .<sup>25</sup> We conduct quasi-static experiments to fit the shear modulus of the elastomer. Figure 2(b) shows the voltage-displacement curve. The black crosses or circles represent the experimental data for a voltage ramp rate of 0.1 kV/s or 0.02 kV/s, respectively, and the dashed blue curve represents the calculations with  $\mu = 562.01$  kPa. As we can see from Fig. 2(b), the elastomer-Oppo band, Singapore exhibits low viscoelasticity. Figure 2(c) shows the displacement of the actuator as a function of time, when we apply a sweeping

$$\Phi = \sqrt{\frac{L_{1A}H}{L_2\varepsilon\lambda_{1A}\lambda_{2p}^2} \left( M \frac{d^2\lambda_{1A}}{dt^2} + c \frac{d\lambda_{1A}}{dt} - \frac{L_2H}{L_{1A}} \mu \left( 2\lambda_{1p} - 2\lambda_{1A} - (2\lambda_{1p} - \lambda_{1A})^{-3} \lambda_{2p}^{-2} + \lambda_{1A}^{-3} \lambda_{2p}^{-2} \right) \right)} = f(\lambda_{1A}), \quad (2)$$

where  $\lambda_{1A} = (L_{1A}\lambda_{1p} + x_d(t))/L_{1A}$ . As shown in Fig. 1(b), first a desired trajectory  $x_d(t)$  is described. Then, the feedforward controller determines the control voltage  $\Phi(t)$ , using Eq. (2) with the identified parameters  $M = 17.5$  g,  $c = 0.696$  Ns/m,  $\mu = 562.01$  kPa, and  $\varepsilon = 2.39 \times 10^{-11} F/m$ . When the voltage is applied to the actuator, the actuator deforms by  $x(d)$ . In what follows, we illustrate how the actuator follows three typical trajectories with triangle, sinusoidal, and stair-like forms. As mentioned above, control of a DEA is the main focus of this paper. Pull-in instability, loss of tension, and electrical breakdown are not analyzed in the present study.

Figure 3 shows the tracking of triangle trajectories. The dashed blue curves in Fig. 3(a) represent the desired triangle trajectories. For each trajectory, the feedforward controller calculates the corresponding control voltage using Eq. (2), as shown in Fig. 3(b). When the voltage is applied to the actuator, the laser sensor measures the actual displacement of the actuator, which is plotted as the solid black curve in Fig. 3(a). Figure 3(c) plots the applied voltage as a function of the experimentally recorded deformation of the actuator. The small hysteresis loop indicates the low viscoelasticity of the elastomer, consistent with Fig. 2(b). The tracking errors are shown in Fig. 3(d). The root-mean-squared errors ( $e_{rms}$ ) are 2.7, 3.2, and 4.2  $\mu m$  for the three trajectories, respectively. As evident in Figs. 3(a) and 3(d), the actuator can track a triangle trajectory with reasonable accuracy.

Figure 4 shows the tracking of sinusoidal trajectories. Frequencies of 0.5 and 5 Hz are selected in this paper since they are close to human haptic perception levels.<sup>21,23</sup> The dashed blue curve in Fig. 4(a) represents the desired sinusoidal trajectory with 0.5 Hz. The control voltage generated by the feedforward controller is shown in Fig. 4(b). The actual displacement of the actuator is shown as the solid black curve in Fig. 4(a). The tracking error is shown in Fig. 4(c).

sinusoidal signal ‘‘Chirp’’ and increase the frequency from 1 Hz to 100 Hz in 10 s. The solid black curve represents the experimental data, and the dashed blue curve represents the calculations. To fit the natural frequency (63.33 Hz), we identify the effective mass  $M = 17.5$  g. To fit the amplitude at resonance (0.16 mm), we identify the damping coefficient  $c = 0.696$  Ns/m. We then verify the dynamic model described by Eq. (1) with the identified parameters by applying a step voltage. Figure 2(d) shows the displacement of the actuator as a function of time. Both the experiments and the simulations are consistent with the settling time (about 0.30 s) and the rising time (about 8 ms, see the inset of Fig. 2(d)).

In this paper, we explore a feedforward controller for deformation control of a DEA by using the above nonlinear dynamic model. Based on (1), we have

Figure 4(d) shows the desired trajectory with a frequency of 5 Hz and the actual displacement of the actuator. Figures 4(e) and 4(f) show the control voltage and the tracking error, respectively. The  $e_{rms}$  are 6.0 and 9.0  $\mu m$  for the trajectories with 0.5 and 5 Hz, respectively. As evident in Figs. 4(a), 4(c), 4(d), and 4(f), the DEA can follow a sinusoidal trajectory with acceptable errors (considering the full displacement range is 110  $\mu m$ ).

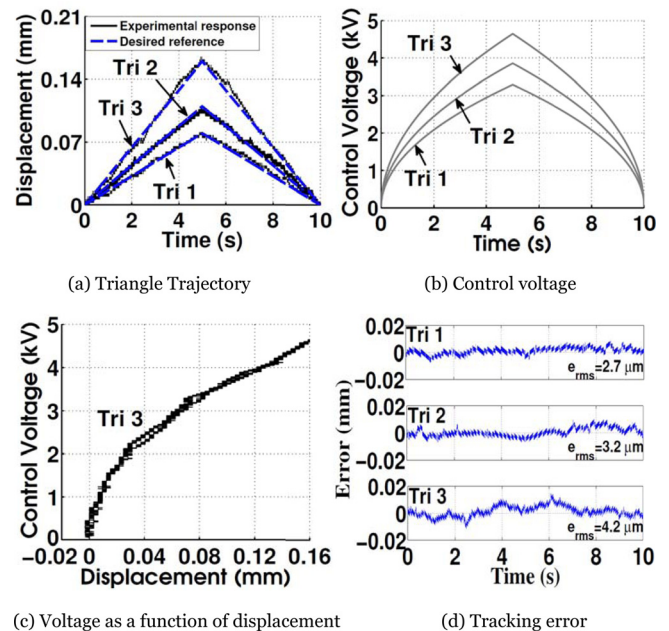


FIG. 3. (a) The triangle trajectories for tracking. The dashed blue curves represent the desired trajectories, while the solid black curves represent the actual displacements of the actuator. (b) Control voltage generated by the feedforward controller. (c) The applied voltage as a function of the experimentally recorded displacement, which shows the small hysteresis loop. (d) Tracking errors.

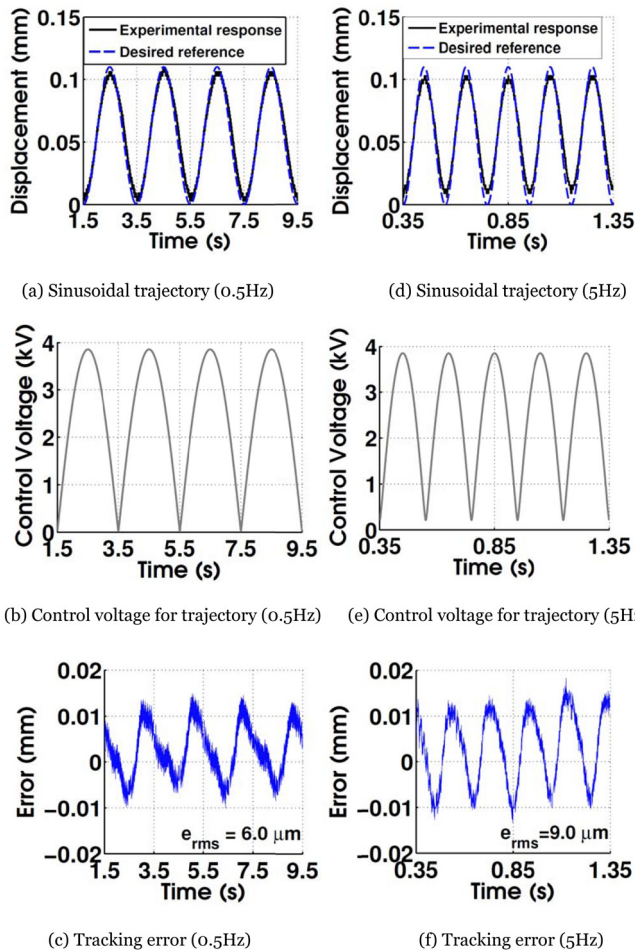


FIG. 4. (a) The sinusoidal trajectory (0.5Hz) for tracking. The dashed blue curve represents the desired trajectory, while the solid black curve represents the actual displacement of the actuator. (b) Control voltage (0.5 Hz). (c) Tracking error (0.5 Hz). (d) The sinusoidal trajectory (5 Hz) for tracking. (e) Control voltage (5 Hz). (f) Tracking error (5 Hz).

Figure 5 shows the tracking of a stair-like trajectory. The desired trajectory and the actual displacement of the actuator are shown in Fig. 5(a). The control voltage generated by the feedforward controller is shown in Fig. 5(b). The tracking error is shown in Fig. 5(c). For simplicity, the controller generates stair-like voltage, ignoring the sudden jump of deformation. As a result, the actuator oscillates at the initial stage of each stair-like voltage, as depicted by the black curve in Fig. 5(a). The oscillation disappears after 0.3–0.4 s due to the damping effect. As shown in Fig. 5(c), the tracking error due to oscillation can be relatively larger, while that for the steady state is smaller. For example, at Stair 2, the  $e_{rms}$  is  $11.3 \mu\text{m}$  in the oscillation and  $5.3 \mu\text{m}$  at the steady state, respectively. In general, the actuator can track a stair-like trajectory with reasonable accuracy. To decrease the oscillation induced by the sudden jump of deformation, the active damping/vibration control approaches can be combined with the controller.<sup>30</sup> In addition, it is found that viscoelasticity of the elastomer may also induce tracking errors. For example, although the desired displacements are the same for Stairs 2 and 4, the actual displacement at Stair 4 is larger than that at Stair 2. This observation is consistent with the hysteresis loop as shown in Fig. 3(c). It is expected that the controller which takes into account the viscoelastic effect can improve the control effect.

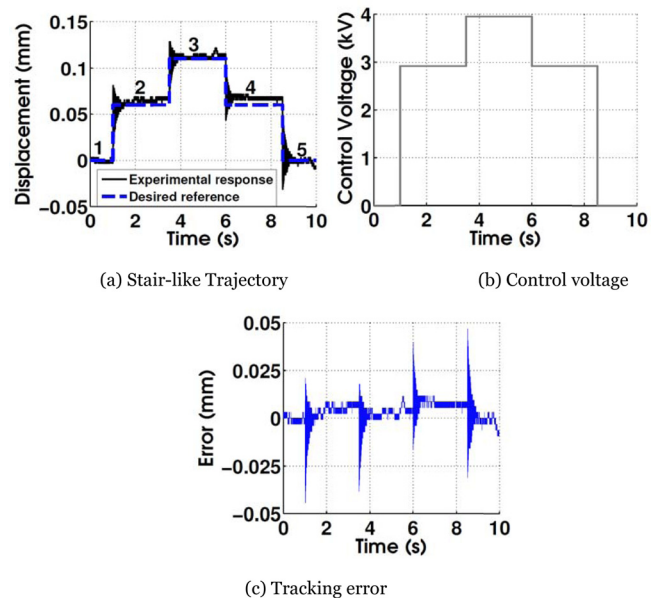


FIG. 5. (a) The stair-like trajectory for tracking. The dashed blue curve represents the desired trajectory, while the solid black curve represents the actual displacement of the actuator. (b) Control voltage generated by the feedforward controller. (c) Tracking error.

The extent to which the controller improves its control accuracy depends on the complexity of the material model. For example, one may want to use several spring and dashpot elements to describe time-dependent behavior of a viscoelastic DEA (say made of VHB).<sup>31</sup>

In summary, this paper investigates feedforward deformation control of a DEA by using a nonlinear dynamic model. The material and physical parameters in the model are identified by quasi-static and dynamic experiments. A feedforward controller is developed based on this nonlinear dynamic model. Experimental evidence shows that this controller can control the DEA to track the desired trajectories effectively. The present study confirms that DEAs are capable of being precisely controlled with the solid dynamic model despite the presence of material nonlinearity and electromechanical coupling. It is expected that the reported results can promote the applications of DEAs to soft robots or biomimetic robots. It should be noted that the present model ignores the strain-stiffening effect and viscoelasticity. When the actuation deformation is large, the dynamic model needs to take into account the strain-stiffening effect. In addition, to improve the control effect, the model needs to consider the viscoelasticity and temporal evolution of the elastomer. Furthermore, the feedback control strategy can be combined with the feedforward controller by considering the modelling uncertainties and external disturbances.

G.G., L.Z., and X.Z. acknowledge support from the National Natural Science Foundation of China (Nos. 51405293 and 51435010), and J.Z. acknowledges support from MOE startup, Singapore (R-265-000-444-133) and MOE Tier 1, Singapore (R-265-000-497-112).

<sup>1</sup>R. Pelrine, R. Kornbluh, Q. B. Pei, and J. Joseph, *Science* **287**, 836 (2000).

<sup>2</sup>S. Ashley, *Sci. Am.* **289**, 52 (2003).

<sup>3</sup>F. Carpi, S. Bauer, and D. De Rossi, *Science* **330**, 1759 (2010).

- <sup>4</sup>P. Brochu and Q. B. Pei, *Macromol. Rapid Commun.* **31**, 10 (2010).
- <sup>5</sup>I. A. Anderson, T. A. Gisby, T. G. McKay, B. M. O'Brien, and E. P. Calius, *J. Appl. Phys.* **112**, 041101 (2012).
- <sup>6</sup>F. Carpi, D. De Rossi, R. Kornbluh, R. Pelrine, and P. Sommer-Larsen, *Dielectric Elastomers as Electromechanical Transducers* (Elsevier, Amsterdam, 2008).
- <sup>7</sup>C. Keplinger, T. F. Li, R. Baumgartner, Z. G. Suo, and S. Bauer, *Soft Matter* **8**, 285 (2012).
- <sup>8</sup>T. F. Li, C. Keplinger, R. Baumgartner, S. Bauer, W. Yang, and Z. G. Suo, *J. Mech. Phys. Solids* **61**, 611 (2013).
- <sup>9</sup>H. Godaba, C. C. Foo, Z. Q. Zhang, B. C. Khoo, and J. Zhu, *Appl. Phys. Lett.* **105**, 112901 (2014).
- <sup>10</sup>C. Keplinger, J. Y. Sun, C. C. Foo, P. Rothmund, G. M. Whitesides, and Z. G. Suo, *Science* **341**, 984 (2013).
- <sup>11</sup>M. Bozlar, C. Punckt, S. Korkut, J. Zhu, C. C. Foo, Z. G. Suo, and I. A. Aksay, *Appl. Phys. Lett.* **101**, 091907 (2012).
- <sup>12</sup>S. M. Ha, W. Yuan, Q. B. Pei, R. Pelrine, and S. Stanford, *Adv. Mater.* **18**, 887 (2006).
- <sup>13</sup>Z. G. Suo and J. Zhu, *Appl. Phys. Lett.* **95**, 232909 (2009).
- <sup>14</sup>J. Zhu, *WW-EAP Newsl.* **17**, 14 (2015).
- <sup>15</sup>R. Krishnan, *Electric Motor Drives: Modeling, Analysis, and Control* (Prentice Hall, New Jersey, 2001).
- <sup>16</sup>J. E. Segel, *Piezoelectric Actuators* (Nova Science Publishers, 2012).
- <sup>17</sup>G. Rizzello, D. Naso, A. York, and S. Seelecke, *IEEE Trans. Control Syst. Technol.* **23**, 632 (2015).
- <sup>18</sup>R. W. Jones and R. Sarban, *Smart Mater. Struct.* **21**, 075019 (2012).
- <sup>19</sup>T. Gisby, E. Calius, S. Xie, and I. A. Anderson, *Proc. SPIE* **6927**, 69271C (2008).
- <sup>20</sup>M. Randazzo, M. Fumagalli, G. Metta, and G. Sandini, *Proc. SPIE* **7642**, 76422D (2010).
- <sup>21</sup>M. Y. Ozsecen and C. Mavroidis, *Proc. SPIE* **7642**, 76422C (2010).
- <sup>22</sup>E. D. Wilson, T. Assaf, M. J. Pearson, J. M. Rossiter, S. R. Anderson, and J. Porri, *Biomimetic Biohybrid Syst.* **8064**, 311 (2013).
- <sup>23</sup>S. Biggs and R. Hitchcock, *Proc. SPIE* **7642**, 76420I (2010).
- <sup>24</sup>U. Gupta, H. Godaba, Z. J. Zhao, C. K. Chui, and J. Zhu, *Extreme Mech. Lett.* **2**, 72 (2015).
- <sup>25</sup>R. Kaltseis, C. Keplinger, S. J. A. Koh, R. Baumgartner, Y. F. Goh, W. H. Ng, A. Kogler, A. Trols, C. C. Foo, Z. G. Suo, and S. Bauer, *RSC Adv.* **4**, 27905 (2014).
- <sup>26</sup>T. F. Li, S. X. Qu, and W. Yang, *Int. J. Solids Struct.* **49**, 3754 (2012).
- <sup>27</sup>Z. G. Suo, *Acta Mech. Solida Sin.* **23**, 549 (2010).
- <sup>28</sup>D. W. Jordan and P. Smith, *Non-linear Ordinary Differential Equations* (Clarendon Press, Oxford, 1987).
- <sup>29</sup>A. H. Nayfeh and D. T. Mook, *Non-linear Oscillation* (Wiley, New York, 1979).
- <sup>30</sup>B. Babakhani, T. de Vries, and J. van Amerongen, *IEEE/ASME Trans. Mechatron.* **18**, 905 (2013).
- <sup>31</sup>M. Kolloosche, G. Kofod, Z. G. Suo, and J. Zhu, *J. Mech. Phys. Solids* **76**, 47 (2015).